www.czasopisma.pan.pl PAN www.journals.pan.pl
Chemical and Process Engineering 2022, 43 (3), 383–404
DOI: 10.24425/cpe.2022.142281

Effect of calcinated halloysite on structure and properties of rigid poly(vinyl chloride) composites

Martina Wieczorek[1], Jolanta Tomaszewska[1*], Tomasz Bajda[2], Jacek Długosz[3]

[1]Bydgoszcz University of Science and Technology, Faculty of Chemical Technology and Engineering, Al. Prof. S. Kaliskiego 7, 85-796 Bydgoszcz, Poland

[2]AGH University of Science and Technology, Faculty of Geology, Geophysics and Environmental Protection, Al. A. Mickiewicza 30, 30-059, Kraków, Poland

[3]Bydgoszcz University of Science and Technology, Faculty of Agriculture and Biotechnology, Al. Prof. S. Kaliskiego 7, 85-796 Bydgoszcz, Poland

Halloysite is a filler which may be used to produce composites with thermoplastic polymer matrix. This work summarized the results of investigations of processing, structural, mechanical, and thermal properties of the composites with poly(vinyl chloride) (PVC) matrix and raw halloysite (HA) as well as its calcined product (KHA). The effectiveness of calcination was confirmed with X-ray diffraction, Fourier-transform infrared spectroscopy, scanning electron microscopy, and nitrogen adsorption method. The PVC composites with HA as well as KHA were processed in the molten state in the Brabender mixer chamber. The reduction of gelation time and simultaneous increase in maximum torque with filler content were found based on the results of plastographometric analysis. SEM images of PVC/halloysite composites showed a homogeneous distribution of the filler in the polymer matrix. The introduction of halloysite leads to a slight increase in Young's modulus and tensile strength compared to neat PVC, where the increase of both parameters is greater when KHA is used. The incorporation of 1% KHA led to an increase in impact strength, an effect which may be attributed to toughening of the polymer. A slight improvement of the Vicat softening temperature of 2.7 °C for PVC/HA and heat deflection temperature of 2.4 °C for PVC/KHA was also ascertained for PVC modified with 10 wt% of filler.

Keywords: polymer composites, mechanical properties, thermal properties, halloysite, poly(vinyl chloride)

1. INTRODUCTION

Halloysite is one of the naturally occurring clay minerals belonging to the kaolinite group. It can form spheroidal, tubular, lamellar, and irregular structures and the diversity of its particle morphology depends on crystallisation conditions. Among the kaolinite group minerals, halloysite is distinguished by the presence of a water monolayer in the inter-pack space (Joussein et al., 2005). Halloysite in its dehydrated form is a 1:1 layered dioctahedral mineral from the kaolin group with a basic chemical composition of $Al_2Si_2O_5(OH)_4$.

* Corresponding author, e-mail: jolanta.tomaszewska@pbs.edu.pl

The layers are composed of silicon tetrahedral and aluminium octahedral sheets that are combined so that the oxygen at the apex of the silicon tetrahedrons extends into and is part of the octahedral sheet. In turn, the layers are held by hydrogen bonds formed between tetrahedral basal oxygens and inner surface hydroxyls of the octahedral sheet.

The layers included in the composition of the packs are negatively charged, thanks to which it is possible to bond cations with their surface and with the edges of the packs (Zahidah et al., 2017). Due to the large variety of charges on the surface of the halloysite, it can be selectively modified, depending on the potential use of the material. Functionalisation of halloysite nanotubes allows to use them, among others, in the production of membranes applied for separation of impurities (Bai et al., 2021), in catalytic reactions (Daraie et al., 2021), and as a material for biomedical engineering (Akrami-Hasan-Kohal et al., 2020). Because of its unique structure, halloysite is used as a filler for plastics, to improve their thermal and mechanical properties (Buruga et al., 2018; De Silva et al., 2016; Deng et al., 2008; Gaaz et al., 2017; Legocka et al., 2013; Liu et al., 2011; 2012; 2013a; 2014a; Liu et al., 2014b; Mondragón et al., 2009; Nakamura et al., 2012; Pasbakhsh et al., 2010b; Yin and Hakkarainen, 2011).

Nakamura et al. (2012) reported that the addition of a 5% mass fraction of halloysite nanotubes (HNT) to bio-based composites comprising jute fabric and soy protein concentrate has a positive effect on flame resistance. Moreover, it was found that Young's modulus of green composites increased with HNT loading up to 10% whereas bending properties were not affected by HNT. A favourable impact of halloysite on thermal stability and tensile strength was confirmed by Buruga et al. (2018) for polystyrene in the form of solution-cast membranes for water purification. The reinforcement effect of halloysite in the form of nanotubes due to their large aspect ratio was found in the case of epoxy nanocomposites, where noticeable enhancements in strength and modulus, as well as fracture toughness, were noted (Deng et al., 2008). Increases in modulus of elasticity and tensile strength were also found in the case of extruded polyamide composites containing halloysite modified with gelatine (Legocka et al., 2013). Halloysite nanotubes modified by γ-methacryloxypropyl trimethoxysilane contributed to an increase in the tensile strength and tensile modulus at 100% elongation values of the ethylene propylene diene monomer (EPDM) (Pasbakhsh et al., 2010a). In the case of poly(lactic acid) nanocomposites, apart from the improvement of the mechanical properties, a favourable effect of halloysite on their thermal stability was found (De Silva et al., 2016).

Halloysite was also applied for the preparation of poly(vinyl chloride)-based composites (Liu et al., 2011; 2012; 2013a; 2014a; Mondragón et al., 2009; Yin and Hakkarainen, 2011). According to Yin and Hakkarainen (2011), PVC films containing HNT nanoparticles surface-grafted with poly(butylene adipate) (PBA) exhibited considerably higher values of modulus and strain at break compared to PVC with unmodified halloysite nanoparticles. Modified HNT could be applied to simultaneously improve the toughness and stiffness of the materials. However, it requires optimisation of the number of PBA chains and their molecular mass. Based on TGA, Liu et al. (2013a) found an improvement in thermal stability of composites containing up to 40 wt% of unmodified halloysite PVC matrix, especially in the first stage of degradation. Introduction of HNTs having hollow tubular structures effectively delayed the degradation process of PVC by interfering with the formation of the conjugated polyene sequences. Moreover, the addition of HNTs led to a remarkable improvement in flame retardancy compared to that of unfilled PVC. In the case of PVC/halloysite nanotubes, nanocomposites synthesised by *in situ* dispersion polymerisation of vinyl chloride in the presence of HNTs, an increase in the notched Izod impact strength with the loading of HNTs up to 4 wt% was found. Increasing the concentration to 6 wt% led to a decrease of the Izod impact energy. A similar tendency was found in the case of tensile strength and flexural strength, while the flexural modulus of the PVC/HNTs nanocomposites increased with the HNTs content. The results indicate that introduction of HNTs leads to an enhancement of stiffness and toughness of PVC when the addition of HNTs is 4.0 wt% or less (Liu et al., 2014a). The increase of the notched Izod impact strength of PVC/HNTs nanocomposites, prepared by melt blending, with the loading of HNTs in the amount of 10% was noted. Increasing the filler concentration to 20, 30 and 40% causes a systematic reduction of the impact toughness, the value of which, however, is higher than that of pure PVC. The values of the tensile

and flexural strength and flexural modulus increased together with the filler's concentration increasing to 40% and were remarkably larger compared with those of the unfilled PVC. These results showed that HNTs were effective in toughening and reinforcing PVC nanocomposites, similarly as described in (Liu et al., 2012). Mondragón et al. (2009) reported also the influence of HNTs in the loading of up to 8% on the mechanical properties of PVC composites and stated that both Izod impact and tensile strength were similar to those of pure PVC while stiffness was reduced with an increase in the HNTs content. In another publication, Liu et al. (2011) found that the polymethyl methacrylate-grafted halloysite nanotubes uniformly dispersed in PVC effectively improved the toughness, tensile and flexural strength and flexural modulus of PVC when added in an amount of up to 5 phr. Additionally, HNT particles cause restraining the thermal motion of PVC molecular chains, leading to a slight improvement of thermal stability.

Obtaining favourable properties of polymer composites containing clay minerals is in many cases related to a modification of the mineral to increase their specific surface area, improve the interaction at the filler-matrix interface and change the nature of the mineral's surface from hydrophilic to hydrophobic (Ghadiri et al., 2015; Goda et al., 2018; Lazorenko et al., 2018; Liu et al., 2014b). Many methods for modification of halloysite are described in the literature, including the application of surface active agents (Abhinayaa et al., 2019; Cavallaro et al., 2016; Lee and Kim, 2002), coupling agents in a grafting reaction (Carli et al., 2014; Luo et al., 2011; Sun et al., 2015; Yuan et al., 2008), by reaction with an ionic monomer (Jiang et al., 2017), as well as by intercalation (Frost and Kristof, 1997; Zhang et al., 2019; Zhang et al., 2020b) and calcination (Tan et al., 2016; Yuan et al., 2012; Zhang et al., 2020a). The calcination of halloysite generates changes in the crystal structure of the mineral, increasing its specific surface area as well as the volume and size of the pores, and thus the adsorption capacity (Deng et al., 2019). During heating of the material in the temperature range of 40–200 °C, dehydration takes place, followed by dehydroxylation which occurs at calcination temperatures from ~500 °C to ~900 °C leading to a loss of long-range order and increasing disconnection of the silica and alumina originally in the tetrahedral and octahedral sheets, respectively. Above the temperature of 600 °C, the formation of amorphous metahalloysite occurs, while between the temperature of 900 °C and 1000 °C, the transformation of halloysite into mullite begins, which leads to the deformation of the nanotubes and reduction of the porosity of the material. First changes in the morphology may be observed at a temperature above 600 °C (Yuan et al., 2012). Deng et al. (2019) reported that precalcination at 800 °C before acid treatment had little effect on the halloysite's tubular morphology, but it improved the halloysite's affinity for benzene molecules due to the dehydroxylation. According to Pajdak et al. (2020), the calcination process carried out at 600 °C caused the development of the pore space of the halloysite and the opening of the smallest mesopores thus the adsorption properties of CO_2 and CH_4 were improved.

There are many reports regarding the calcination of natural halloysite (Deng et al., 2019; Pajdak et al., 2020; Yuan et al., 2012; Zhang et al., 2020a). However, the available literature lacks reports on the impact of the natural halloysite calcination process on the mechanical and thermal properties of composites based on large-tonnage polymers, including poly(vinyl chloride), which belongs to the commonly used polymers due to favourable properties, such as relatively low price, widely developed processing, environmental resistance and possibilities of modification of properties.

The goal of our research was to obtain composites with a homogeneous dispersion of halloysite in a matrix of unplasticised poly(vinyl chloride) by melt blending, which should allow to obtain a new composite material with favourable mechanical and thermal properties. Halloysite has been modified by the calcination method to rise its hydrophobic properties favouring an increase in the interactions with the polymer matrix. Subsequently, structure (by scanning electron microscopy) as well as processing, mechanical (tensile strength, elongation at break, Young modulus and impact strength), and thermal properties (softening and heat deflection temperature, Congo red test) of composites containing calcined halloysite were performed and compared with those for composite with non-modified halloysite.

This research provides new knowledge concerning the development of innovative PVC-based composite engineering materials with mineral filler.

2. EXPERIMENTAL

2.1. Materials

For the preparation of composites, a dry blend composed of dispersion of PVC S-61 Neralit (Spolana Anwil Group, Neratovice, Czech Republic) 100 phr, organotin stabilizer Patstab 2310 (Patcham, Goor, the Netherlands) 4 phr, and 1 phr Naftolube FTP paraffin wax (Chemson, Arnoldstein, Austria) was used. The stabilizer and the paraffin wax were the only added components to minimise the influence of additives on processing properties. As a filler, halloysite in the form of a powder (HA) collected from Polish deposit Dunino, located in the SW part of Poland near Legnica, and halloysite modified by calcination (KHA) were used. The Dunino deposit, covering an area of 1.99 ha, was documented in 1996. Halloysite from this deposit is a product of the weathering of tertiary basalt rocks. It has the form of a horizontal seam, is homogeneous in composition, and was included in the second group of deposit variability in accordance with the Baryszew classification (average variability) (Lutyński et al., 2019). The thickness of the deposit ranges from 3.5 to 18.8 m (average 12.2 m). The measured resources of this deposit are 470.63 thousand t, whereas proven reserves account for 374.66 thousand t (Lutyński et al., 2019). The Dunino deposit is characterised by a homogeneous composition. The predominant part of the profile comprises a zone of halloysite composition, in which the proportion of kaolinite is 1–10%, and subordinate occurrences of goethite, illite, and montmorillonite (Stoch et al., 1977).

2.2. Methods of halloysite characterisation

XRD analysis was conducted on a SmartLab RIGAKU diffractometer using a copper X-ray tube, in the angular range of 2–70°2θ with a 0.05°2θ measuring step. The phases were identified based on the results using the X-RAYAN computer software (Version 4.2.2, "KOMA", Warsaw, Poland).

The structure of raw and calcined halloysite was also determined using Fourier-transform infrared spectroscopy (FTIR). The study was carried out using an Alpha apparatus from Bruker, by the ATR (reflective) technique, in the range of 4000–360 cm^{-1}, two scans at a resolution of 2 cm^{-1} were applied.

The morphology of the halloysite was observed using a scanning electron microscope (JEOL 6480LV, JEOL Ltd., Tokyo, Japan) equipped with an energy-dispersive X-ray spectrometer for elemental microanalysis (EDS). The samples were observed in the low-vacuum mode (LV-SEM) using a backscattered electron detector (BSE) at 1Pa of chamber pressure, under an acceleration voltage of 20 kV and 11 mm working distance. The EDS analyses were conducted for 5 samples of raw halloysite.

Characteristics of the porous texture of unmodified halloysite and calcinated halloysite were determined based on isotherms of low-temperature nitrogen adsorption and desorption at a temperature of –196 °C. The analysis was carried out using an apparatus for precise measurements ASAP 2020 (Micromeritics) in a broad range of relative pressures of approximately 10^{-3} to 0.99. Before the measurement, the sample was annealed in vacuo at a temperature of 110 °C for 12 h. The following parameters of porous texture were evaluated:

1. Specific surface area according to Brunauer–Emmet–Teller (BET) method.
2. Total volume of the pores $V_{tot}^{0,99}$ for a relative pressure of $\frac{p}{p^0} = 0.99$.
3. Volume of micropores V_{mik}^{DR} (pores having a width smaller than 2 nm) according to the Dubinin–Radushkevich method.
4. Volume of mesopores V_{mez}^{BJH} (pores having a width larger than 2 nm and smaller than 50 nm) according to Barrett–Joyner–Halenda (BJH) method.

The analysis of porous texture was performed according to the recommendations of the following standards: ISO 9277:2010(E), ISO 15901-2:2006(E), ISO 15901-3:2007(E), and NIST 2006.

2.3. Preparation of PVC composites with HA and KHA

Powder mixtures of poly(vinyl chloride) with the raw halloysite and separately with the calcined halloysite were prepared by mixing with a high shear mixer. Before processing, the halloysite was dried at 105 °C for 3 h. The PVC dry blend and PVC compounds containing 1 wt%, 5 wt%, and 10 wt% of unmodified halloysite and halloysite after calcination were processed by kneading in a Brabender type FDO 234H plastographometer with the temperature of chamber walls of 185 °C, using a rotation speed of the main rotor of 30 rpm, with the friction of 1:1.5. The charge weight was 60 g in each case. The kneading of the PVC dry blend and each PVC-halloysite mixture was performed for 10 minutes and repeated 5 times, obtaining a total of 300 g of the processed material. The compositions of the PVC mixtures and their abbreviations as used in the text are presented in Table 1.

Table 1. Compositions of the PVC-based composites

Sample	Filler type	Filler content, wt%
PVC	–	–
PVC/1HA	raw halloysite	1
PVC/5HA		5
PVC/10HA		10
PVC/1KHA	calcinated halloysite	1
PVC/5KHA		5
PVC/10KHA		10

The processed materials were comminuted and then pressed at a temperature of 190 °C under the pressure of 15 MPa, obtaining mouldings with dimensions of 100 × 100 mm and thicknesses of 2 and 4 mm. The ground material was used to determine the thermal stability by the Congo red method. Samples for the static tensile test, impact strength and hardness as well as softening temperature measurements were cut from the mouldings using the Seron 6090 numerical milling plotter (Seron, Poland).

To evaluate the processing properties of the PVC blend and composites with pristine and calcinated halloysite, the torque of the rotors was recorded as a function of time during kneading. From the obtained plastograms, the values characterising the processing properties were read, i.e. the maximum value of the torque (M_X) and the time of its achievement (t_X), as well as the torque at equilibrium (M_E) according to the methodology described in our previous papers (Tomaszewska et al., 2007; Mirowski et al., 2021) as well as in (Liu et al., 2014a; Liu et al., 2012).

2.4. Testing methods of PVC composites with HA and KHA

To determine the structure of composites, the observations of PVC composites with 1 wt% of filler were carried out using scanning electron microscopy (JEOL 6480LV, JEOL Ltd., Tokyo, Japan). The samples for the SEM observations were fractured in liquid nitrogen and sputtered with a thin layer of gold-palladium. The observations were made using a voltage of 20 kV.

Thermal stability was determined by the Congo red method; the test was carried out at a temperature of 200 °C according to the ISO 182-1:1990 standard.

The Vicat softening point tests were carried out on samples with dimensions of 10 mm × 10 mm × 4 mm according to the ISO 306:2006 standard using a Ceast HDT Vicat Tester HV3. For every sample type, the measurements were done in triplicate.

The heat deflection temperature (HDT) was determined according to the ISO 75-1:2020 standard using a Ceast HDT Vicat Tester HV3. The heating rate was 2 °C/min and the applied load was 1.8 MPa. The samples were measured flatwise with a 64 mm span distance.

The Charpy impact strength without notch was tested using a HIT5P device from Zwick Roell (Zwick GmbH & Co. KG, Ulm, Germany) according to the ISO 179-2:2010 standard.

D-type Shore hardness tests were carried out using an apparatus from Zwick Roell (Zwick GmbH & Co. KG, Ulm, Germany) according to the ISO 868:2003 standard.

The static tensile test was carried out using a Zwick Roell Z010 universal testing machine (Zwick GmbH & Co. KG, Ulm, Germany) according to the ISO 527-1:2012, using type 1BA samples (overall length 78 mm, the distance between broad parallel-sided portions 59 mm, length of narrow parallel-sided portion 30 mm, gauge length 25 mm, width at narrow portion 5.0 mm, width at ends 10 mm, thickness 2 mm). The test was carried out at room temperature using the tensile rate of 1 mm/min in the range of modulus of elasticity determination and then 30 mm/min. Modulus of elasticity (E_t), stress at yield (σ_Y), tensile strength (σ_M) and strain at break (ε_B) were determined. The measurements were carried out for ten samples of each material.

Observations of the failure surfaces of PVC composites after tensile tests were carried out using a Hitachi FlexSEM1000 scanning electron microscope (Hitachi Ltd., Tokyo, Japan) operating with a voltage of 20 kV. The samples were observed in the variable-pressure mode (VP-SEM) using a BSE-COMP detector, at 40 Pa of chamber pressure, and a 9.6 mm working distance.

3. RESULTS AND DISCUSSION

3.1. Preparation of halloysite

In the first step, two grain fractions were separated from halloysite by sieve analysis: below 50 μm (fraction 1) and above 50 μm (fraction 2). For further studies, only halloysite fraction 1 was used. Analysis of particle size was carried out to determine actual grain sizes. Grain size distribution of halloysite in the range of 0.18 to 100 μm was determined by sedimentation in an aqueous environment using a Sedigraph III X-ray analyser (Micromeritics Instrument Corporation, Norcross, GA, USA). The dispersion for measurements was prepared using 20 g of the sample and 80 ml of 0.20% sodium metaphosphate solution in distilled water as a dispersion medium. The whole system was mixed with a magnetic stirrer for 24 hours.

Based on the grain size distribution, it was found that fraction 1 contained 96% of particles having an average size of 2 μm (Fig. 1).

In the next step, particles of halloysite fraction 1 were calcinated in a dryer from Binder company, at a temperature of 800 °C for 2 h. Conditions of calcination were defined based on (Zhang et al., 2020a), where the optimal temperature of the process is approx. 750 °C to ensure a high degree of dihydroxylation. The time required for noticeable structural changes to occur is approx. 2 hours.

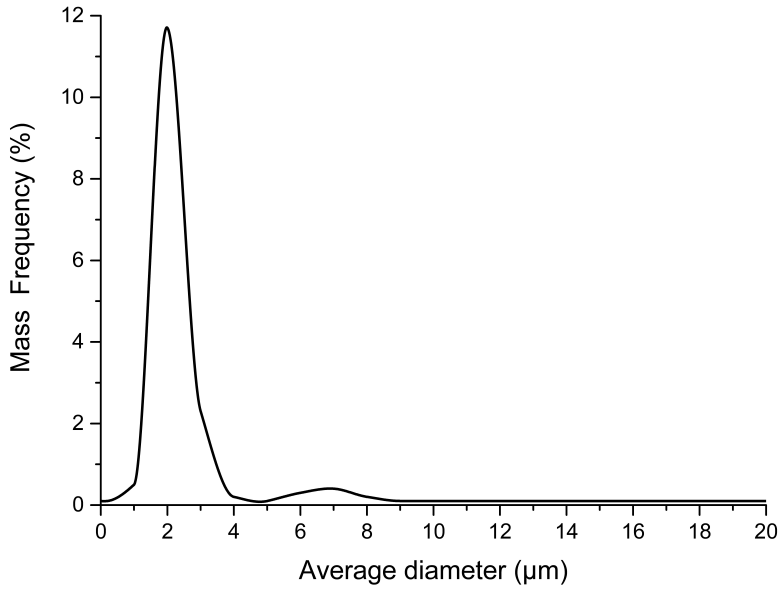

Fig. 1. Particle-size distribution of halloysite fraction 1

3.2. Effectiveness of halloysite modification

3.2.1. XRD analysis

Figure 2 shows a diffractogram of raw halloysite (HA) and calcined halloysite (KHA). The XRD patterns of HA showed a basal characteristic reflection at 7.34 Å, which is attributed to dehydrated halloysite (7 Å). Other reflections (4.43 Å, 2.56 Å, 2.35 Å, 2.23 Å, 1.67 Å) confirm the structure of the halloysite. In the HA sample, apart from halloysite, there is also kaolinite (4.44 Å, 4.17 Å, 3.61 Å, 1.49 Å), as well as a trace

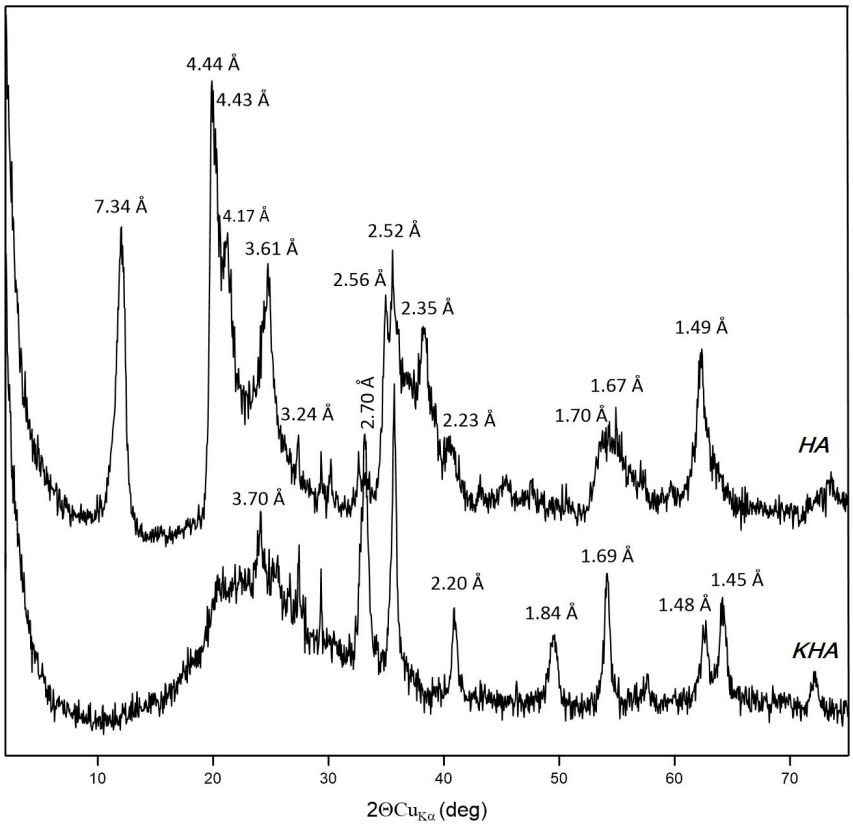

Fig. 2. XRD patterns of HA and KHA

amount of iron oxides (maghemite – 2.52 Å; hematite – 1.70 Å) and feldspars (3.24 Å). In the calcination process, the structure of halloysite and kaolinite is dehydroxylated. Hence the KHA sample diffractogram shows no reflections from these minerals. The patterns of KHA show broad diffraction maxima (10–30°2θ) owing to dehydroxylation and formation of an X-ray amorphous product, metahalloysite (Lutynski et al., 2019). The remaining reflections in the KHA sample diffraction pattern originate from hematite (3.70 Å, 2.70 Å, 2.20 Å, 1.84 Å, 1.69 Å, 1.48 Å, 1.45 Å).

3.2.2. FTIR analysis

FTIR spectra for halloysite and calcinated halloysite are shown in Fig. 3. The 1106 cm^{-1} band, characteristic for halloysite, may be attributed to the in-plane Si–O stretching vibration. The oscillations at 1031 cm^{-1} correspond to valence vibrations in the Si–O–Si plane.

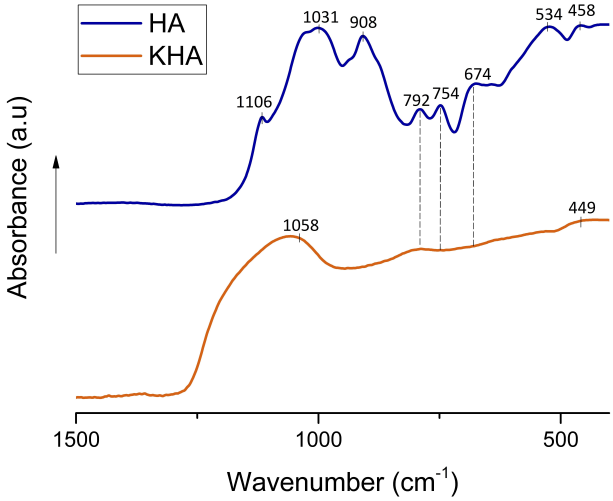

Fig. 3. FTIR absorbance spectra of halloysite (HA) and calcined halloysite (KHA)

The band at 908 cm^{-1} corresponds to internal vibrations of AlOH hydroxyl groups. The band at 792 cm^{-1} may be attributed to Si–O symmetric stretching. The band at 754 cm^{-1} corresponds to Si–O perpendicular stretching. The Al–O oscillations at 674 cm^{-1} are connected with five coordinated aluminium atoms. The oscillations at 534 cm^{-1} are caused by Al–O–Si deformation. On the other hand, the oscillations at 458 cm^{-1} originate from Si–O–Si deformation.

The bands at 1106 cm^{-1} and 1031 cm^{-1} in the halloysite sample are split. When the temperature increases, halloysite forms a disordered structure, which causes a shift of the 1031 cm^{-1} band towards higher wavenumbers, 1058 cm^{-1}. A lack of band at 908 cm^{-1} in the KHA spectrum confirms the dehydroxylation process resulting from the heating of the halloysite. The band at 792 cm^{-1} and 754 cm^{-1}, despite its lower intensity, has the same location as that in the halloysite not subjected to calcination. It may be caused by the decay of the ordered lattice of Si_2O_5 and the separation of silica and alumina. This phenomenon is supported also by the lack of the band at 534 cm^{-1}, which has been connected with the Al–O–Si deformation. Broadening and shift of the band corresponding with Si–O–Si vibrations at 458 cm^{-1} towards lower numbers result from the calcination process. In this case, the average Si–O–Si bond angle connected with the disturbance of the mineral system increases (Yuan et al., 2012; Zhang et al., 2020a).

3.2.3. SEM observations

The morphology of raw halloysite and calcinated halloysite was characterized by SEM, as shown in Figure 4. In the case of non-calcinated HA, lamellar structure prevails, and agglomerates of nanoparticles of various forms, including nanotubes, are visible. These structure elements with sizes from 5 to 10 μm

are present on the whole SEM image (Figures 4a and 4b). Lutyński et al. (2019) proved a simultaneous presence of halloysite nanoplates and nanotubes in samples of halloysite from the Dunino mine. It can therefore be assumed that these structures are also present in the halloysite samples used in our study, but in Figures 4a and 4b the individual nanoparticles are invisible due to formation of agglomerates.

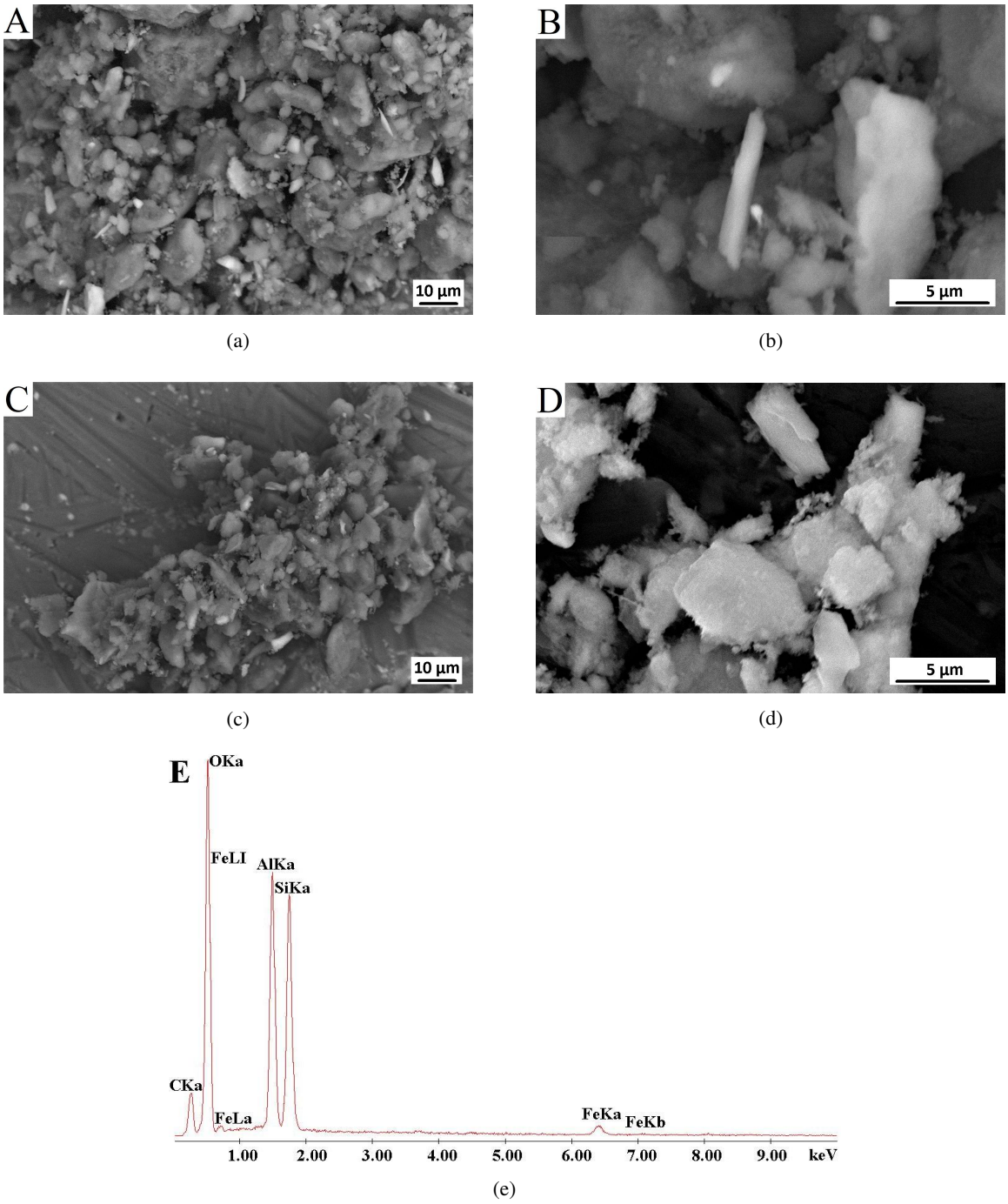

Fig. 4. SEM images of raw halloysite (a, b), calcined halloysite (c, d) and EDS spectrum (e)

On the other hand, calcinated halloysite is characterised by a lamellar-angular structure. A significant part of the aggregates cannot be considered as plates because of their thickness (Figs. 4c and 4d). As in the case of HA, the presence of individual agglomerates of nanoparticles with dimensions of 5–10 µm may be found. However, there are clearly fewer of them compared to the sample of raw halloysite and the diameter of the agglomerates present on the SEM image is slightly smaller; structure elements with a size of 1–2 µm are also visible.

Based on Deng et al. (2019) and Tironi et al. (2017), a breach of the tubular structure occurs when the temperature exceeds 900 °C; thus, it can be assumed that the structure of the agglomerate-forming nanotubes has not changed due to calcination in our experiment.

The EDS spectrum of the raw halloysite seen in Fig. 4e confirms that aluminium, silicon and oxygen are the basic elements constituting the mineral. Also, a reflection indicating the presence of iron is evident in the EDS spectrum, in agreement with (Lutyński et al., 2019); an iron oxide impurity was also found based on electron energy loss spectroscopy spectrum (Filice et al., 2021).

3.2.4. Texture analysis

The results of texture analysis of HA and KHA samples are presented in Table 2. The specific surface area of unmodified halloysite amounts to 73.2 m^2/g.

Table 2. Parameters of porous texture of raw and calcinated halloysite

Sample	S_{BET} [m^2/g]	$V_{tot}^{0.99}$ [cm^3/g]	V_{mik}^{DR} [cm^3/g]	V_{mez}^{BJH} [cm^3/g]
HA	73.2	0.184	0.028	0.136
KHA	40.7	0.197	0.017	0.155

The literature data indicate that the BET surface area of halloysite depends on (similarly to its mineralogy, chemical composition, and physicochemical properties) the localisation of halloysite ore deposit and amounts to, according to various sources, from 24.2 m^2/g to 65 m^2/g (Lvov the et al., 2008; Sun et al., 2015; Zhang et al., 2012), while according to (Joussein, 2016), from 22.10 m^2/g to 74.6 or even 81.6 m^2/g (Liu et al., 2014b).

The data presented in Table 2 show that the specific surface area of the calcined halloysite is much smaller than that of the raw halloysite and amounts to 40 m^2/g. It may be caused by a smaller share of the tubular structure, as well as a change from lamellar to lamellar-angular with larger dimensions of this structure, which is confirmed by the results of SEM observations. The change in the structure and size of its elements is also proved by a significant increase in the total volume of pores and a decrease in the volume of micropores accompanied by a simultaneous increase in the volume of mesopores.

A similar effect of reduction of the specific surface area resulting from the halloysite calcination was described in the publication (Deng et al., 2019). The specific surface area of raw halloysite was 58.4 m^2/g, and calcination at a temperature of 800 °C resulted in its decrease to 54.4 m^2/g. Zhang et al. (2020a) suggest that this effect is connected with the destruction or degradation of tubular structures caused by calcination, although such structural changes usually take place at a temperature of 1000 °C or even higher. A different effect of calcination of halloysite originating from the same deposit is described in (Yuan et al., 2012), where the samples were annealed at a temperature from 120 to 1400 °C and then ground into powders. It was found that the specific surface area of halloysite annealed at a temperature of 120 °C amounted to 72.5 m^2/g and increased to 78.1 m^2/g in the case of halloysite calcinated at a temperature of 900 °C. Temperature increase above 1000 °C caused a decrease in specific surface area and porosity due to substantial collapse of the tubular structure occurred or formation of large mullite particles under sintering.

According to Pajdak et al. (2020) an increase in the specific surface area, resulting from calcination was ascertained for halloysite originating from the Dunino mine, when the specific surface area of raw halloysite amounted to 62.7 m^2/g, while that of halloysite calcinated at a temperature of 600 °C was 69.8 m^2/g.

The total volume of pores of raw halloysite is 0.184 cm^3/g, that of micropores 0.028 cm^3/g, and that of mesopores 0.136 cm^3/g. In the case of calcinated halloysite, the total volume of pores increased to 0.197 cm^3/g. The effect of an increase in the total volume of pores in halloysite originating from the Dunino mine was described also by Pajdak et al. (2020); the value of V_{tot} for the mineral without thermal treatment amounted to 0.096 cm^3/g, while after calcination it was 0.185 cm^3/g. In turn, Deng et al. (2019) proved that the total volume of pores of raw halloysite was 0.27 cm^3/g, and after calcination at a temperature of 800 °C, it decreased to 0.202 cm^3/g.

According to Sun et al. (2015), the total volume of pores of unmodified halloysite was only 0.08 cm^3/g and it increased to 0.11 cm^3/g due to activating treatment using piranha solution.

Based on our results and literature data (Pasbakhsh et al., 2013; Zhang et al., 2012), it may be ascertained that the features of the halloysite structure, i.e. pore volume and specific surface area, depend not only on the type and conditions of treatment but most of all, on the origin of halloysite and the related morphological features. In the case of the HA sample, lamellar structure prevails, and nanotubes rarely, whereas in the case of KHA, a lamellar-angular structure. The lamellar morphology results in a looser texture and consequently, a larger specific surface area (Table 2) than in the case of the more compact, closed lamellar-angular structure.

3.3. Processing properties of PVC/halloysite composites

During the processing of PVC, most often carried out by the extrusion method, a transformation of grains form into a compact form of the final product occurs. This transformation is called PVC gelation which follows by the action of heat, pressure and shear and consists of the gradual disintegration of PVC grains, their plasticization and fusion. The conditions of gelation determine not only the obtaining of a product with a homogeneous structure and therefore favourable properties, but also the effective operation of thermal stabilizers. To characterize the progress in PVC gelation in processing conditions, the torque measurements during kneading in a Brabender or Haake rheometer chamber are used. These measurements make it possible to record the time-dependent changes of the torque in the form of plastograms.

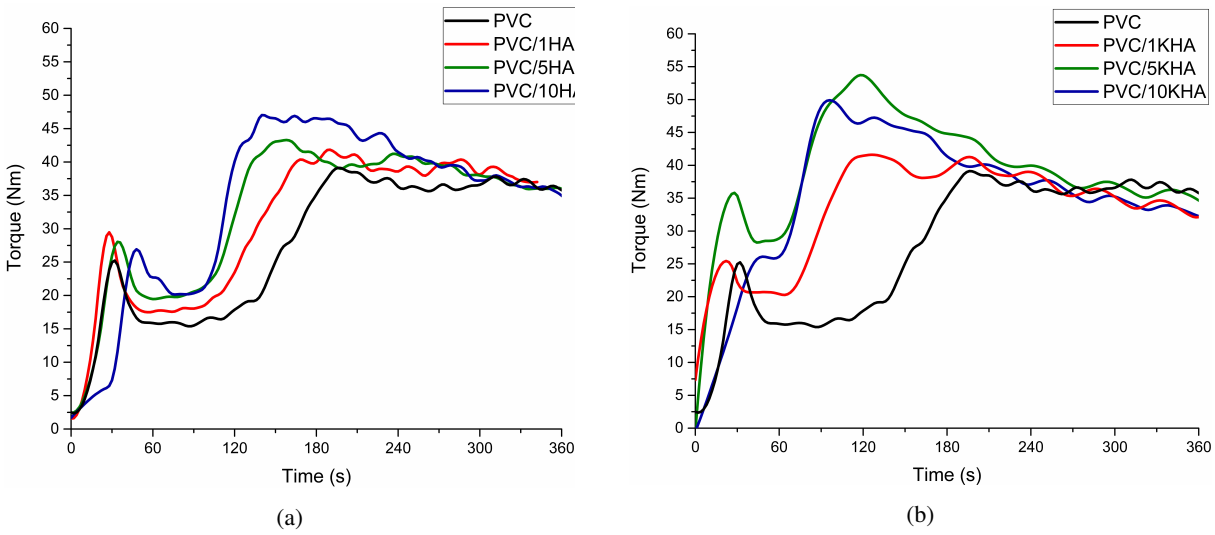

Fig. 5. Torque vs. time of kneading for PVC and PVC composites with HA (a) and KHA (b)

The course of the plastograms illustrated in Fig. 5 is similar and typical for non-plasticised PVC blends. The first smaller torque maximum observed in the plastograms is related to the feeding of the chamber. The further course of the plastograms, which show a clear maximum of torque, proves that the kneading

conditions (i.e. temperature, the rotational speed of the rotors and the mass of the batch) are correctly selected. These conditions determine the proper transformation of the morphological structure of the initial PVC grains and the formation of a molten mixture in the final kneading stage (Shubbar, 2011; Tomaszewska et al., 2007).

Compared to unfilled PVC, the maximum values of torque (M_X) related to gelation of PVC matrix are higher for mixtures containing both unmodified and calcined halloysite (Table 3). The M_X values increase with the concentration of the filler in mixtures; in the case of 10 wt% of filler content, they are higher by approx. 27% for PVC/KHA and by approx. 20% for PVC/HA compared to unfilled PVC. Differences in the M_X values of PVC/HA and PVC/KHA mixtures were observed, particularly when the filler content equalled 5 wt%. The torque values in the equilibrium state of mixtures of PVC with unmodified and calcinated halloysite are also higher compared to unfilled PVC, although the changes in the M_E value as a function of the filler concentration are not as significant as in the case of the maximum torque. Simultaneously, the time of reaching the maximum value of the torque decreased with the increase in the concentration of the filler, regardless of its type. The shortest gelation time was found for the mixture containing 10 wt% of calcined halloysite where t_X is almost twice as short compared to pristine PVC. The observed effects are related to the increased friction of filler particles against one another or against PVC grains, of PVC grains against one another, or of filler particles or PVC grains against the surface of the chamber wall, generating additional heat (Tomaszewska et al., 2007). Due to these effects, the gelation of PVC with fillers is faster than that of PVC, especially in the case of PVC/KHA. A similar effect of shortening the gelation time with a simultaneous increase in the maximum torque was reported by Liu et al. (2012) for PVC/HNTs nanocomposites prepared with direct melt mixing. The authors claimed that the introduction of HNTs to the PVC matrix can result in higher frictional energy and shorten the time to absorb the required energy for the PVC particles to fuse together.

Table 3. Plastographometric analysis of PVC and PVC composites with HA and KHA

Sample	t_X [min]	M_X [Nm]	M_E [Nm]
PVC	3.5 (0.4)	40.0 (0.6)	36.0 (0.6)
PVC/1HA	3.3 (0.5)	42.8 (0.9)	37.5 (1.5)
PVC/5HA	2.7 (0.5)	43.9 (0.8)	36.4 (1.3)
PVC/10HA	2.5 (0.4)	47.9 (1.0)	34.3 (1.1)
PVC/1KHA	3.0 (0.6)	43.1 (1.0)	38.1 (1.2)
PVC/5KHA	2.0 (0.2)	54.1 (0.9)	36.1 (1.0)
PVC/10KHA	1.7 (0.1)	50.8 (1.1)	34.6 (0.4)

A different effect was reported in another work by Liu et al. (2014a) for PVC/HNTs nanocomposites synthesised via *in situ* polymerisation and then processed in a molten state where the plasticisation time was found to be longer than that of the neat PVC. Simultaneously, the equilibrium torque and the maximum torque of PVC/HNTs nanocomposites were found to be increased with increasing HNTs content suggesting that the processability of the nanocomposites is worse than that of pure PVC. These observations are consistent with the results of plastographometric tests presented in this paper and described in our earlier paper for PVC with hybrid silica/lignin filler (Klapiszewski et al., 2015) and PVC with various types of natural fillers (Mengeloglu and Matuana, 2003; Mirowski et al., 2021; Tomaszewska et al., 2017).

3.4. Structure of PVC/halloysite composites

To evaluate the effect of thermal treatment of halloysite on the distribution of particles in the polymeric matrix, SEM observations of the fracture surfaces of the composite samples containing 1 wt% of HA and KHA were carried out.

The fracture surface of both samples (Figs. 6a–6d) shows evenly dispersed particles smaller than 0.5 μm and individual spherical filler particles of about 1 μm embedded in the polymer matrix. The spherical particle visible in Fig. 6d with a size of ca. 2 μm is probably an iron oxide particle, the numerous presence of which on the surface of the platy structures in halloysite samples from the Dunino mine was confirmed in (Filice et al., 2021). Single particles of filler are stably "embedded" in the polymer matrix, but there are also visible voids on the surface, from which the filler has most likely been torn out during breaking. Comparing the micrographs of the composites PVC/HA and PVC/KHA it can be seen that there are fewer voids on the surface of the composite containing KHA (Figs. 6c, 6d), which may indicate an improvement in the interaction at polymer–filler interface due to calcination of the filler.

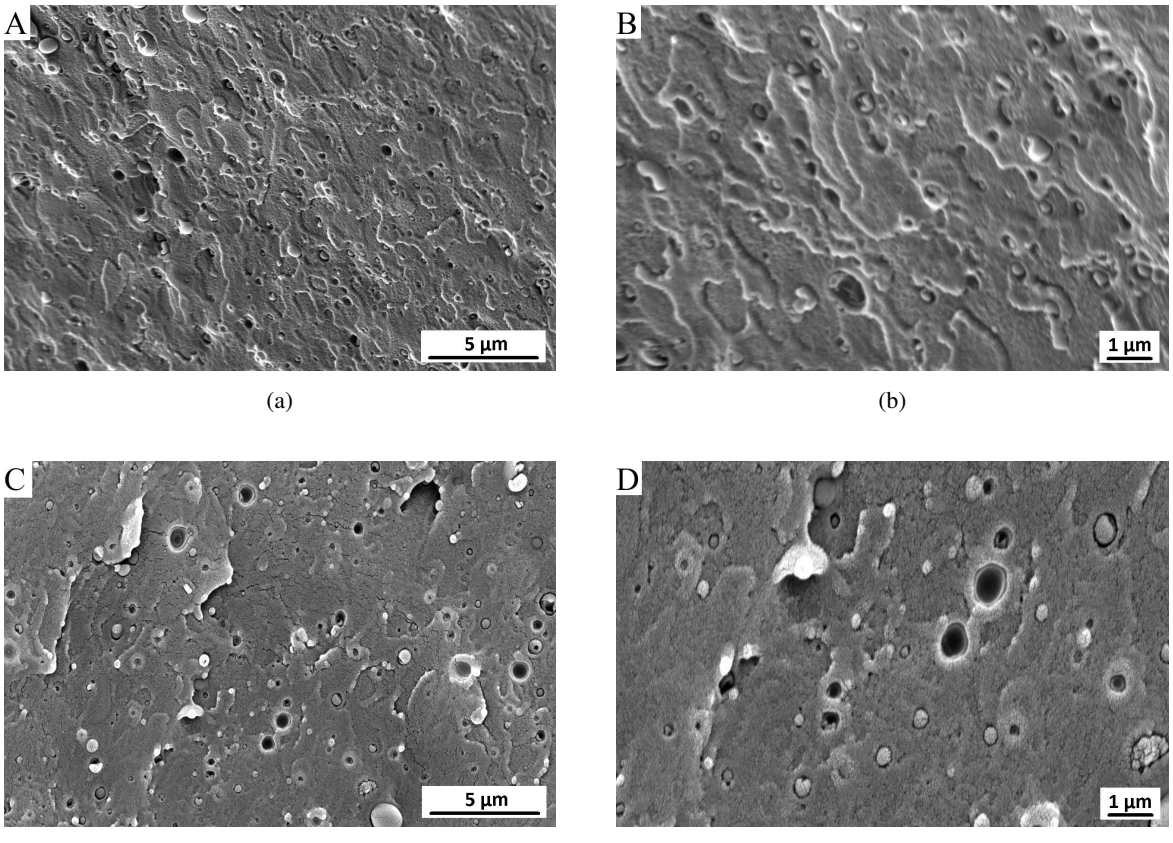

(a) (b)

(c) (d)

Fig. 6. SEM micrographs of the fracture surfaces of PVC composites: PVC/1HA (a, b); PVC/1KHA (c, d)

3.5. Thermal properties

The results of thermal stability tests using the Congo red method, the Vicat softening temperature (VST) and the heat deflection temperature (HDT) of PVC and composites on PVC matrix with HA and KHA are presented in Table 4. A slight improvement (by 1min) in thermal stability compared to the unmodified polymer was only found for the composite containing 1 wt% of calcined halloysite; the same content of unmodified halloysite did not affect the thermal stability. Increasing the filler content to 5 wt% resulted in a slight decrease in stability (by 3 min) for raw HA composites and only by 1 min for those containing

KHA. Composites containing 10 wt% of fillers are characterised by the lowest thermal stability, whereby the deterioration of stability is slightly less (by 1min) in the case of composites with unmodified halloysite.

Table 4. Thermal properties of PVC and PVC composites with HA and KHA

Sample	Thermal stability [min]	Vicat softening temperature [°C]	Heat deflection temperature [°C]
PVC	18 (1.0)	79.3 (0.2)	64.5 (0.2)
PVC/1HA	18 (0.5)	79.9 (0.3)	65.0 (0.3)
PVC/5HA	15 (0.5)	80.8 (0.4)	65.5 (0.3)
PVC/10HA	11 (0.5)	82.0 (0.4)	66.3 (0.2)
PVC/1KHA	19 (0.5)	80.7 (0.1)	65.1 (0.5)
PVC/5KHA	17 (1.0)	81.2 (0.3)	65.9 (0.1)
PVC/10KHA	12 (0.5)	81.2 (0.4)	66.9 (0.4)

A slight improvement in thermal stability was found for PVC composites containing up to 5 wt% poly(methyl methacrylate)-grafted halloysite nanotubes (HNTs) (Liu et al., 2011). Liu et al. stated that well-dispersed HNTs restrict the long-range chains mobility of PVC and may act as a barrier, hindering the permeability of volatile degradation products. In another paper by the same Authors, TGA measurements indicated that the halloysite nanotubes in concentrations up to 40 wt% enhance the heat resistance of PVC (Liu et al., 2013a). A different thermal effect than that found in our research (Liu et al., 2011; Liu et al., 2013a) may be connected with another morphological structure of halloysite particle, as well as chemical composition and amount of impurities, among others, iron oxides (iron(II) and iron(III)), in comparison to halloysite applied in our work. At processing temperature, iron oxides react with HCl evolving as a consequence of dehydrochlorination of PVC to form $FeCl_2$ and $FeCl_3$, which promotes a further degradation process (Girois, 1999).

The analysis of the results of the Vicat softening temperature (Table 4) shows that its value is higher by approx. 1–2 °C for composites containing halloysite as compared to unmodified PVC. No significant effect of halloysite modification on the VST value was found. A similar trend was found for the heat deflection temperature (HDT), the value of which for the composite containing 10 wt% of calcined halloysite was 2.4 °C higher compared to that of pure PVC. A similar increase in the HDT, compared to the unfilled PVC, was observed for composites containing halloysite nanotubes, where the introduction of 2 and 4 wt% of the filler caused an increase in heat deflection temperature by 2 °C compared to that of unfilled PVC (Liu et al., 2014a).

A favourable effect of halloysite on thermal properties was also found in the case of composites based on other thermoplastic polymers, including polylactide matrix (Liu et al., 2013b), which was connected with homogeneous distribution and orientation of the filler in the polymer matrix. Meanwhile, Sikora et al. (2019) found that the addition of halloysite nanotubes reduced the Vicat softening point of composites on a low-density polyethylene matrix. It should be mentioned that microscopic observations of PE/HNT composites showed the presence of numerous agglomerates of the filler proving a poor dispersion in the polymer matrix. According to Sikora et al. (2019), HNT increases the thermal resistance of composites only when it is evenly dispersed in the polymer matrix.

3.6. Mechanical properties

The results of studies on the mechanical properties of PVC and composites with unmodified and calcined fillers are presented in Table 5. The impact strength (a_{cU}) of composite with 1 wt% of raw halloysite is similar to that of pure poly(vinyl chloride) and decreases along with increasing concentration of filler in the PVC matrix up to 8.9 kJ/m^2 for 10 wt% of HA.

Table 5. Mechanical properties of PVC as well as PVC/HA and PVC/KHA composites

Sample	H [ShD]	a_{cU} [kJ/m^2]	E_t [MPa]	σ_Y [MPa]	δ_M [MPa]	ε_B [%]
PVC	77.6 (0.2)	15.9 (0.7)	1600 (10)	54.1	54.1 (0.2)	23.2 (0.9)
PVC/1HA	77.9 (0.3)	15.8 (1.0)	1610 (15)	–	52.8 (0.4)	8.0 (1.7)
PVC/5HA	78.7 (0.1)	11.6 (0.6)	1660 (12)	–	49.2 (0.8)	3.9 (1.2)
PVC/10HA	79.6 (0.2)	8.9 (1.0)	1750 (17)	–	44.3 (1.0)	3.4 (0.8)
PVC/1KHA	78.5 (0.5)	23.3 (1.2)	1670 (10)	55.8	55.8 (0.4)	22.0 (1.2)
PVC/5KHA	79.3 (0.2)	13.8 (0.8)	1730 (12)	53.4	53.4 (1.0)	15.4 (0.8)
PVC/10KHA	80.1 (0.1)	7.8 (0.8)	1860 (14)	56.0	56.0 (0.5)	6.6 (1.5)

Thermal treatment of halloysite affected the impact strength of composites beneficially. The composite containing 1 wt% KHA was characterised by the highest impact strength; its value was about 47% higher compared to that of unmodified PVC and a composite with the same amount of unmodified halloysite. On the contrary, with increasing content of KHA, the a_{cU} value decreases, reaching the lowest value for composites with 10% of the filler (7.8 kJ/m^2), similarly as in the case of PVC/HA.

Liu et al. (2012) found an improvement in the Izod impact strength of PVC composites containing up to 10 wt% of halloysite filler, which is related to good dispersion of nanoparticles with the low hydroxyl density on the surface. The well-dispersed particles changed the stress state of the matrix material and induced the deformation of PVC, which absorbs the impact energy and prevents the initiation of cracks. According to Liu et al. (2012), the decrease in the impact strength of the composites with a high content of filler (up to 30%) is related to a decrease in the distances between the particles which aggregate and act as stress concentrators leading to a decrease in the toughness of the polymer matrix. The results of the notched Izod impact strength measurements of PVC/HNTs nanocomposites prepared by two-stage method (by *in situ* polymerisation and then, by processing in molten state) indicate that as the nanoparticles loading is increased to 4.0 wt%, the Izod impact energy reaches a maximum and the improvement is 36% compared to pure PVC (Liu et al., 2014a). The influence of the homogeneity of the halloysite distribution in the matrix on the impact strength was confirmed by Mondragón et al. (2009), ascertaining its deterioration in the case of composites based on PVC containing up to 8 wt% of the filler, due to ineffective stress transfer to the halloysite.

The use of both raw and calcinated halloysite leads to an increase in the hardness (H) of composites compared to unmodified PVC; H values of composites with 10 wt% of filler are higher by 2.6% for PVC/HA and by 3.2% if KHA introduced into the matrix.

The mechanical stress-strain curves of PVC, PVC/HA and PVC/KHA composites with various contents of fillers are presented in Figure 7. In the case of neat PVC, a ductile-type fracture accompanied by a significant plastic deformation was noted. Similar stress-strain behaviours are observed for PVC with calcinated halloysite. A clear yield point appears in the curve where its value represents the tensile strength

($\delta_Y = \delta_M$). In the case of samples of PVC/HA, a transformation from ductile to brittle-like fracture was observed, and consequently, the yield point disappeared.

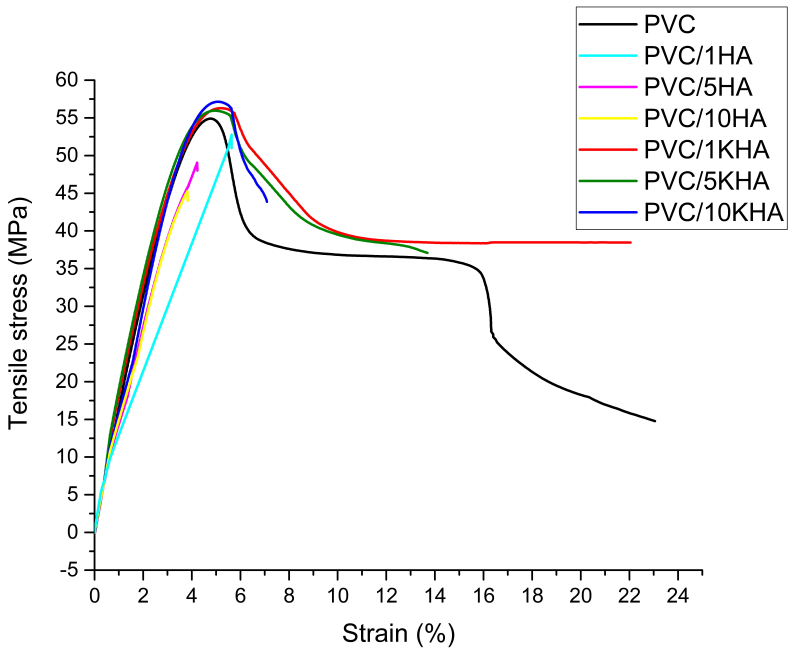

Fig. 7. Stress-strain curves of PVC composites with various loading of HA and KHA

The values of mechanical properties summarised in Table 5 indicate that the introduction of halloysite, regardless of the type, leads to an increase in Young's modulus compared to neat PVC, where the E_t value growths along with an increase in the filler's concentration in the polymer matrix.

The data presented in Table 5 show that for the same filler concentration, Young's modulus is higher in the case of composites containing previously thermally treated halloysite. For composites containing 10% of the filler, the modulus value is higher compared to unmodified PVC by 9.4% for PVC/HA composites and by 16.3% when calcined halloysite was introduced into the matrix. The values of tensile strength of PVC/KHA composites are slightly higher compared to those of unfilled PVC and there is practically no dependence on the filler concentration (Table 5). On the other hand, all PVC/HA samples are characterised by a lower tensile strength than pristine PVC and its value decreases with increasing concentration of the filler in the matrix; a 10% share of HA causes a decrease in δ_M by approx. 20% compared to PVC. Elongation at break revealed the highest value for pure PVC (23.2%) and decreased sharply with the increasing raw halloysite content, reaching 3.4% for the composite containing 10% of the filler. The changes in the elongation of PVC/KHA composites as a function of the filler content are different, i.e. the 1% share of KHA practically does not affect ε_B and an increase in the share to 10% results in a reduction of the value to 6.6%.

The presented results of mechanical tests confirm the effectiveness of calcination, as a halloysite surface modification leading to an increase in its hydrophobic properties. It may be assumed that this effect alters the interactions between particles of fillers and the polymer matrix, resulting in an improvement in mechanical properties, especially an increase in Young's modulus, and a minor increase in the strength value along with the increase in the KHA concentration. Moreover, the improvement in mechanical properties is related to the presence of nanostructures in halloysite, which significantly affect the interfacial interactions. The slight increase in Young's modulus is already observed at 1% KHNT content (by approx. 5% compared to pristine PVC), which, with a simultaneous significant increase in impact strength (by approx. 46% compared to unmodified PVC) and an almost identical elongation value, may indicate a simultaneous occurrence of two effects related to the introduction of KHA: toughening and reinforcement. With an increase in KHA content in the matrix, the reinforcement begins to dominate over the toughening effect, because the values of impact strength and elongation decrease, while the E_t values increase, reaching the

maximum value for a composite with 10% KHA content. The toughening effect was not observed for the composites with raw halloysite, whereas an increase in the stiffness of these materials was found with an increase in the HA concentration in the PVC matrix.

Similarly, the beneficial effect of a filler with a surface with hydrophobic properties on the mechanical properties of PVC matrix composites was reported by Zhao et al. (2016). Introduction of up to 10 wt% of calcium carbonate particles modified with surfactant into PVC resulted in a significant increase in impact strength and tensile strength, whose values were much higher in comparison with composites containing unmodified $CaCO_3$ particles with hydrophilic character. The elongation at break was also improved indicating high toughness. Liu et al. (2012) reported the increase in strength as well as modulus of PVC composites related to the satisfactory compatibility of HNTs with polar poly(vinyl chloride). Strong interactions at the interface ensure that the loads are effectively transferred from the polymer to the filler phase. A different effect was observed by Mondragón et al. (2009), finding a decrease in the rigidity of the rigid PVC composites containing up to 8% of halloysite, probably due to the formation of the relatively compliant layer at the interface. An increase in elongation accompanying the decrease in Young's modulus at the content of 3 wt% of the filler probably results from the HNT orientation and simultaneously, from the interfacial viscoelastic deformation.

Although the two effects (reinforcement- toughening) observed in our research related to the introduction of 1 wt% of calcined halloysite into the PVC matrix are reflected in the literature, it should be noted that those described in the papers (Liu et al., 2012; Liu et al., 2014a; Mondragón et al., 2009) concern PVC composites containing the halloysite filler in a significantly higher concentration. The reasons may include the fact that the applied halloysite originated from various deposits, and therefore had a different structure and content of impurities than that used in our research. Additionally, it should be emphasised that the final mechanical properties of polymer composites, including those based on PVC, are determined mainly by the properties of the matrix, which in turn depend on the type of PVC used, the composition of the mixture, and the processing conditions. Apart from the applied filler, these factors significantly affect the properties of composites based on PVC.

An increase in tensile strength, Young's modulus and elongation at break associated with the introduction of halloysite was confirmed among others, during testing of composites based on polyamide, polylactide, poly(lactic-co-glycolic acid), the carboxylated butadiene-styrene rubber, epoxy resin, polycaprolactone, ethylene-propylene-diene rubber, fluoroelastomers and poly(vinyl alcohol) nanocomposite films (Liu et al., 2014b). However, in every case, the improvement of mechanical properties was related to the halloysite nanotubes loading, dispersion, and interfacial interactions in the systems.

Fig. 8 shows SEM micrographs of tensile-fractured surfaces of samples of composites containing 1 wt% of calcined halloysite (Figs. 8a, 8b) and raw halloysite (Figs. 8c, 8d) The images confirm the brittle behaviour found based on the stress-strain curves (Fig. 7) exhibited by the composite samples containing HA and the ductile behaviour characteristic for the samples with KHA. The surface appearance of PVC/HA specimens presented in Figs. 8c and 8d shows brittle failure characteristics, without any appreciable plastic deformation. The surface is relatively smooth, and the rupture has occurred where a cluster of filler particles of about 50 μm and smaller is visible (Fig. 8d). The image also shows individual filler particles in the form of plates.

The ductile nature of the deformation is evidenced by the fibril-like layer structure visible in Fig. 8b. During stretching, as a result of progressive deformation of the matrix, detachment at the particle-polymer interface occurred and, as a consequence, ellipsoidal voids were formed around the filler particles, clearly deformed in the stretching direction (Figs. 8a and 8b). The layers of polymer, in which the filler particles are stably embedded, moving in relation to each other, cause some destruction of the structure of approximal layers of the polymer. The image also shows single filler particles of about 20 μm in size (Fig. 8a), which were not found in the SEM micrographs shown in Figure 6.

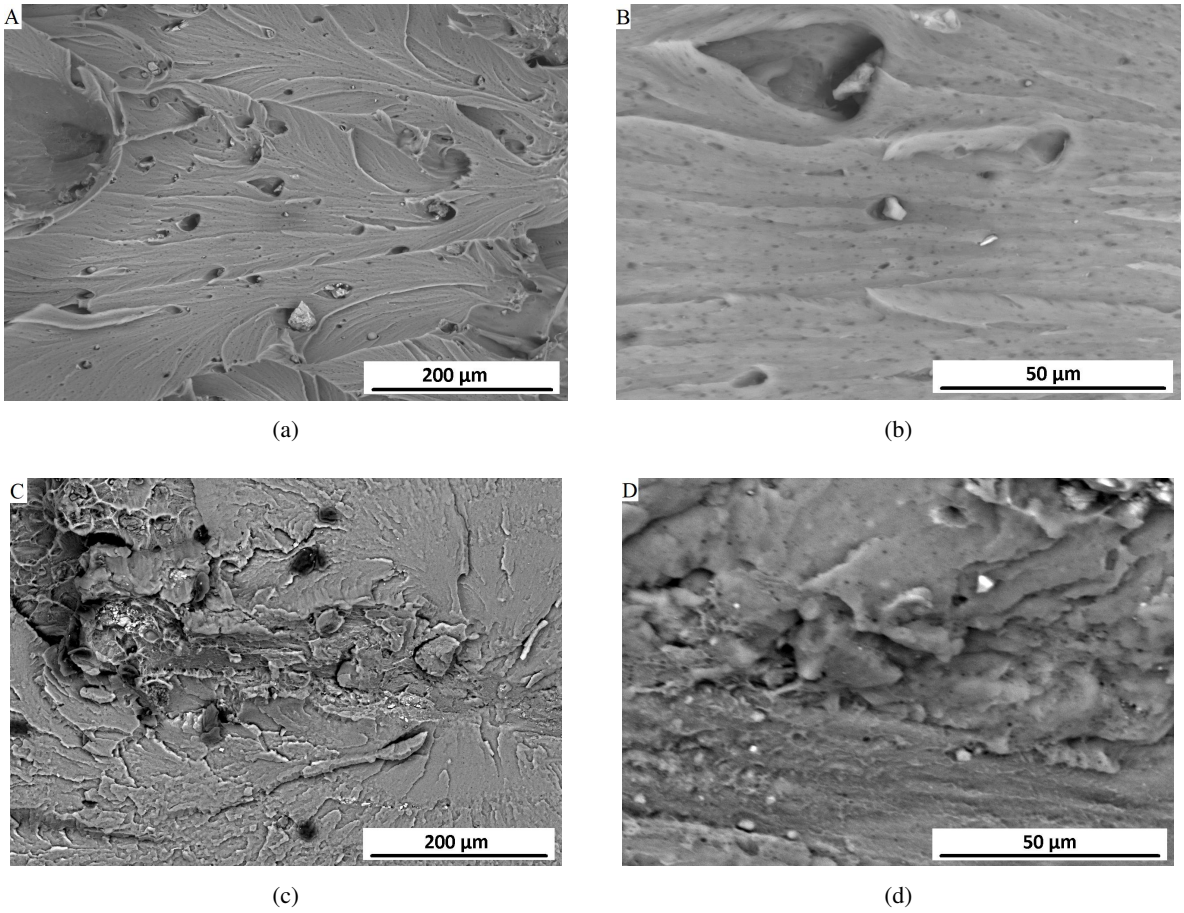

Fig. 8. SEM images of tensile failure surfaces of the PVC composites containing 1 wt% of KHA (a, b) and HA (c, d)

Similar microscopic observations were described by Zhao et al. (2016) for PVC samples containing hydrophobic calcium carbonate nanoparticles. The SEM micrographs of the tensile-fractured surfaces of the composites with 5 wt% of modified filler showed some cavities on the fracture surface. Zhao et al. (2016) also stated that the $CaCO_3$ particles and PVC were combined well and the cavitations could absorb large amounts of energy, leading to the improvement of the composites' tensile strength. Based on SEM micrographs of the impact surfaces of PVC/HNTs composites, Liu et al. (2014a) stated that nanocomposites with 2.0 and 4.0 wt% show ductile characteristics with a rough fracture surface and some cracks. In another publication, the same team evaluated fracture surfaces of broken specimens after an impact test of PVC composites containing 10 phr and 30 phr of HNTs and confirmed a large amount of squamous structure exhibiting plastic shear deformation and ductile behaviours. Observations of SEM of the samples after tensile tests indicate that the PVC matrix in composites containing 3.0 and 10.0 phr of HNTs was largely deformed and drawn around the HNTs particles (Liu et al., 2012).

4. CONCLUSIONS

Halloysite from Dunino deposit may be used to produce composites with unplasticized PVC matrix containing up to 10 wt% of filler using a two steps method of processing in a molten state. The kneading of PVC and halloysite mixtures in properly determining conditions make it possible to obtain rightly gelated composites used for further compression moulding. The reduction of plasticization time and simultaneous increase of maximum torque with filler content were found based on the results of plastographometric

analysis. These effects, more visible in composites containing KHA, are caused by the generation of additional heat due to friction between filler particles and PVC grains.

Introduction of halloysite, both in the form of raw material, as well as modified one, using the calcination method, contributed to a slight increase in the stiffness and hardness of the composites, whereas the increase was slightly bigger in composites with calcined halloysite. Calcination of the filler increased its hydrophobic properties, which resulted in an improvement of the interaction at polymer–filler interface and, as a consequence, in an improvement of the mechanical properties of the composites. The incorporation of 1% KHA led to a simultaneous increase of impact strength which could be attributed to the toughening effect.

Some inconsiderable improvement of softening and heat deflection temperature of the composites in comparison with pristine PVC was also found.

Halloysite from the Dunino mine can be used as a cheap filler of PVC mixtures for the production of new materials with favourable functional properties, especially mechanical ones. The introduction of halloysite to PVC will decrease the costs of the final product with, simultaneously, unchanged or higher mechanical parameters.

The comparison of properties of PVC/HA and PVC/KHA composites shows that the improvement of properties related to the introduction of halloysite subjected to thermal treatment is not as significant as expected.

The authors would like to express the gratitude to Jan Seyda for conducting SEM observations.

REFERENCES

Abhinayaa R., Jeevitha G., Mangalaraj D., Ponpandian N., Meena P., 2019. Toxic influence of pristine and surfactant modified halloysite nanotubes on phytopathogenic bacteria. *Appl. Clay Sci.*, 174, 57–68. DOI: 10.1016/j.clay.2019.03.022.

Akrami-Hasan-Kohal M., Ghorbani M., Mahmoodzadeh F., Nikzad B., 2020. Development of reinforced aldehyde-modified kappa-carrageenan/gelatin film by incorporation of halloysite nanotubes for biomedical applications. *Int. J. Biol. Macromol.*, 160, 669–676. DOI: 10.1016/j.ijbiomac.2020.05.222.

Bai Z., Wang L., Liu C., Yang C., Lin G., Liu S., Jia K., Liu X., 2021. Interfacial coordination mediated surface segregation of halloysite nanotubes to construct a high-flux antifouling membrane for oil-water emulsion separation. *J. Membr. Sci.*, 620, 118828. DOI: 10.1016/j.memsci.2020.118828.

Boudhani H., Lainé C., Fulchiron R., Cassagnau P., 2007. Rheology and gelation kinetics of PVC plastisols. *Rheol. Acta*, 46, 825–838. DOI: 10.1007/s00397-006-0157-4.

Buruga K., Kalathi J.T., Kim K.H., Ok Y.S., Danil B., 2018. Polystyrene-halloysite nano tube membranes for water purification. *J. Ind. Eng. Chem.*, 61, 169–180. DOI: 10.1016/j.jiec.2017.12.014.

Carli L.N., Daitx T.S., Soares G. V., Crespo J.S., Mauler R.S., 2014. The effects of silane coupling agents on the properties of PHBV/halloysite nanocomposites. *Appl. Clay Sci.*, 87, 311–319. DOI: 10.1016/j.clay.2013.11.032.

Cavallaro G., Grillo I., Gradzielski M., Lazzara G., 2016. Structure of hybrid materials based on halloysite nanotubes filled with anionic surfactants. *J. Phys. Chem. C*, 120, 13492–13502. DOI: 10.1021/acs.jpcc.6b01282.

Daraie M., Heravi M.M., Rangraz Y., Besharati Z., 2021. Pd NPs supported on halloysite functionalized with Schiff base as an efficient catalyst for Sonogashira reaction. *Sci. Rep.*, 11, 6223. DOI: 10.1038/s41598-021-85821-2.

De Silva R.T., Soheilmoghaddam M., Goh K.L., Wahit M.U., Hamid S.B.A., Chai S.-P., Pasbakhsh P., 2016. Influence of the processing methods on the properties of poly(lactic acid)/halloysite nanocomposites. *Polym. Compos.*, 37, 861–869. DOI: 10.1002/pc.23244.

Deng L., Yuan P., Liu D., Du P., Zhou J., Wei Y., Song Y., Liu Y., 2019. Effects of calcination and acid treatment on improving benzene adsorption performance of halloysite. *Appl. Clay Sci.*, 181, 105240. DOI: 10.1016/j.clay.2019.105240.

Deng S., Zhang J., Ye L., Wu J., 2008. Toughening epoxies with halloysite nanotubes. *Polymer*, 49, 5119–5127. DOI: 10.1016/j.polymer.2008.09.027.

Filice S., Bongiorno C., Libertino S., Compagnini G., Gradon L., Iannazzo D., La Magna A., Scalese S., 2021. Structural characterization and adsorption properties of Dunino raw halloysite mineral for dye removal from water. *Materials*, 14, 3676. DOI: 10.3390/ma14133676.

Frost R.L., Kristof J., 1997. Intercalation of halloysite: A Raman spectroscopic study. *Clays Clay Miner.*, 45, 551–563. DOI: 10.1346/CCMN.1997.0450407.

Gaaz T.S., Sulong A.B., Kadhum A.A.H., Al-Amiery A.A., Nassir M.H., Jaaz A.H., 2017. The impact of halloysite on the thermo-mechanical properties of polymer composites. *Molecules*, 22, 838. DOI: 10.3390/molecules 22050838.

Ghadiri M., Chrzanowski W., Rohanizadeh R., 2015. Biomedical applications of cationic clay minerals. *RSC Adv.*, 5, 29467–29481. DOI: 10.1039/C4RA16945J.

Girois S., 1999. Effect of iron compounds (oxide, salt, or complexes) on poly(vinyl chloride) thermal and photochemical stability. *J. Vinyl Add. Tech.*, 5, 218–230. DOI: 10.1002/vnl.10335.

Goda E.S., Yoon K.R., El-sayed S.H., Hong S.E., 2018. Halloysite nanotubes as smart flame retardant and economic reinforcing materials: A review. *Thermochim. Acta*, 669, 173–184. DOI: 10.1016/j.tca.2018.09.017.

Jiang Y., Wang P., Zheng J., 2017. Use of ionic monomers to prepare halloysite polymer nanocomposites with reinforced mechanical performance. *Appl. Clay Sci.*, 141, 248–256. DOI: 10.1016/j.clay.2017.03.003.

Joussein E., 2016. Geology and mineralogy of nanosized tubular halloysite. *Developments in Clay Science*, 7, 12–48. DOI: 10.1016/B978-0-08-100293-3.00002-9.

Joussein E., Petit S., Churchman J., Theng B., Righi D., Delvaux B., 2005. Halloysite clay minerals — a review. *Clay Miner.*, 40, 383–426. DOI: 10.1180/0009855054040180.

Klapiszewski Ł., Pawlak F., Tomaszewska J., Jesionowski T., 2015. Preparation and characterization of novel PVC/silica-lignin composites. *Polymers*, 7, 1767–1788. DOI: 10.3390/polym7091482.

Lazorenko G., Kasprzhitskii A., Yavna V., 2018. Synthesis and structural characterization of betaine- and imidazoline-based organoclays. *Chem. Phys. Lett.*, 692, 264–270. DOI: 10.1016/j.cplett.2017.12.054.

Lee S.Y., Kim S.J., 2002. Adsorption of naphthalene by HDTMA modified kaolinite and halloysite. *Appl. Clay Sci.*, 22, 55–63. DOI: 10.1016/S0169-1317(02)00113-8.

Legocka I., Wierzbicka E., Al-Zahari T.M., Osawaru O., 2013. Influence of halloysite on the structure, thermal and mechanical properties of polyamide 6. *Polimery*, 58, 24–32. DOI: 10.14314/polimery.2013.024.

Liu C., Luo Y., Jia Z., Li S., Guo B., Jia D., 2012. Structure and properties of poly(vinyl chloride)/halloysite nanotubes nanocomposites. *J. Macromol. Sci. Part B Phys.*, 51, 968–981. DOI: 10.1080/00222348.2011.564106.

Liu C., Luo Y., Jia Z., Li S., Huang D., Jia D., 2014a. Particle configuration and properties of poly(vinyl chloride)/halloysite nanotubes nanocomposites via in situ suspension polymerization. *Polym. Compos.*, 35, 856–863. DOI: 10.1002/pc.22729.

Liu C., Luo Y.F., Jia Z.X., Zhong B.C., Li S.Q., Guo B.C., Jia D.M., 2013a. Thermal degradation behaviors of poly(vinyl chloride)/halloysite nanotubes nanocomposites. *Int. J. Polym. Mater. Polym. Biomater.*, 62, 128–132. DOI: 10.1080/00914037.2011.617328.

Liu C., Luo Y.F., Jia Z.X., Zhong B.C., Li S.Q., Guo B.C., Jia D.M., 2011. Enhancement of mechanical properties of poly(vinyl chloride) with polymethyl methacrylate-grafted halloysite nanotube. *eXPRESS Polym. Lett.*, 5, 591–603. DOI: 10.3144/expresspolymlett.2011.58.

Liu M., Jia Z., Jia D., Zhoua C., 2014b. Recent advance in research on halloysite nanotubes-polymer nanocomposite. *Prog. Polym. Sci.*, 39, 1498–1525. DOI: 10.1016/j.progpolymsci.2014.04.004.

Liu M., Zhang Y., Zhou C., 2013b. Nanocomposites of halloysite and polylactide. *Appl. Clay Sci.*, 75–76, 52–59. DOI: 10.1016/j.clay.2013.02.019.

Luo P., Zhang J.S., Zhang B., Wang J.H., Zhao Y.F., Liu J.D., 2011. Preparation and characterization of silane coupling agent modified halloysite for Cr(VI) removal. *Ind. Eng. Chem. Res.*, 50, 10246–10252. DOI: 10.1021/ie200951n.

Lutyński M., Sakiewicz P., Lutyńska S., 2019. Characterization of diatomaceous earth and halloysite resources of Poland. *Minerals*, 9, 670. DOI: 10.3390/min9110670.

Lvov Y.M., Shchukin D.G., Möhwald H., Price R.R., 2008. Halloysite clay nanotubes for controlled release of protective agents. *ACS Nano*, 2, 814–820. DOI: 10.1021/nn800259q.

Mengeloglu F., Matuana L.M., 2003. Mechanical properties of extrusion-foamed rigid PVC/wood- flour composites. *J. Vinyl Addit. Technol.*, 9, 26–31. DOI: 10.1002/vnl.10058.

Mirowski J., Oliwa R., Oleksy M., Tomaszewska J., Ryszkowska J., Budzik G., 2021. Poly(vinyl chloride) composites with raspberry pomace filler. *Polymers*, 13, 1079. DOI: 10.3390/polym13071079.

Mondragón M., Roblero-Linares Y.S., Sánchez –Espíndola M.E., Zendejas-Leal B.E., 2009. Rigid poly(vinyl chloride)/ halloysite nanocomposites, In: Laudon M., Romanowicz B. (Eds.), *NSTI Nanotech 2009 Proceedings*, Vol. 3: Nanotechnology 2009, 482–484.

Nakamura R., Netravali A.N., Morgan A.B., Nyden M.R., Gilman J.W., 2012. Effect of halloysite nanotubes on mechanical properties and flammability of soy protein based green composites. *Fire Mater.*, 37, 75–90. DOI: 10.1002/fam.2113.

Pajdak A., Skoczylas N., Szymanek A., Lutyński M., Sakiewicz P., 2020. Sorption of CO_2 and CH_4 on raw and calcined halloysite-structural and pore characterization study. *Materials*, 13, 917. DOI: 10.3390/ma13040917.

Pasbakhsh P., Churchman G.J., Keeling J.L., 2013. Characterisation of properties of various halloysites relevant to their use as nanotubes and microfibre fillers. *Appl. Clay Sci.*, 74, 47–57. DOI: 10.1016/j.clay.2012.06.014.

Pasbakhsh P., Ismail H., Ahmad Fauzi M.N., Bakar A.A., 2010a. EPDM/modified halloysite nanocomposites. *Appl. Clay Sci.*, 48, 405–413. DOI: 10.1016/j.clay.2010.01.015.

Pasbakhsh P., Ismail H., M.N., Ahmad Fauzi M.N., Bakar A.A., 2010b. Halloysite nanotubes as a novel nanofiller for polymer nanocomposites. *Extended Abstracts – 21st Australian Clay Minerals Conference – Brisbane, August 2010*. 93–96.

Shubbar S.D.A., 2011. The effect of shear on the properties of rigid PVC. *J. Eng.*, 17, 1567–1575.

Sikora J.W., Gajdoš I., Puszka A., 2019. Polyethylene-matrix composites with halloysite nanotubes with enhanced physical/thermal properties. *Polymers*, 11, 787. DOI: 10.3390/polym11050787.

Stoch L., Dyjor S., Kalmus S., Sikora W., 1977. *Zwietrzeliny bazaltowe Dolnego Śląska*. Prace Mineralogiczne, 56. Zakład Narodowy im. Ossolińskich, Wrocław.

Sun P., Liu G., Lv D., Dong X., Wu J., Wang D., 2015. Effective activation of halloysite nanotubes by piranha solution for amine modification *via* silane coupling chemistry. *RSC Adv.*, 5, 52916–52925. DOI: 10.1039/c5ra04444h.

Tan D., Yuan P., Liu D., Du P., 2016. Surface modifications of halloysite. *Developments in Clay Science*, 7, 167–201. DOI: 10.1016/B978-0-08-100293-3.00008-X.

Tironi A., Cravero F., Scian A.N., Irassar E.F., 2017. Pozzolanic activity of calcined halloysite-rich kaolinitic clays. *Appl. Clay Sci.*, 147, 11–18. DOI: 10.1016/j.clay.2017.07.018.

Tomaszewska J., Klapiszewski Ł., Skórczewska K., Szalaty T.J., Jesionowski T., 2017. Advanced organic-inorganic hybrid fillers as functional additives for poly(vinyl chloride). *Polimery*, 62, 19–26. DOI: 10.14314/polimery.2017.019.

Tomaszewska J., Sterzyński T., Piszczek K., 2007. Rigid poly(vinyl chloride) gelation in a brabender measuring mixer. III. Transformation in the torque maximum. *J. Appl. Polym. Sci.*, 106, 3158–3164. DOI: 10.1002/app.26754.

Yin B., Hakkarainen M., 2011. Core-shell nanoparticle-plasticizers for design of high-performance polymeric materials with improved stiffness and toughness. *J. Mater. Chem.*, 21, 8670–8677. DOI: 10.1039/c1jm10624d.

Yuan P., Southon P.D., Liu Z., Green M.E.R., Hook J.M., Antill S.J., Kepert C.J., 2008. Functionalization of halloysite clay nanotubes by grafting with γ-aminopropyltriethoxysilane. *J. Phys. Chem. C*, 112, 15742–15751. DOI: 10.1021/jp805657t.

Yuan P., Tan D., Annabi-Bergaya F., Yan W., Fan M., Liu D., He H., 2012. Changes in structure, morphology, porosity, and surface activity of mesoporous halloysite nanotubes under heating. *Clays Clay Miner.*, 60, 561–573. DOI: 10.1346/CCMN.2012.0600602.

Zahidah K.A., Kakooei S., Ismail M.C., Raja P.B., 2017. Halloysite nanotubes as nanocontainer for smart coating application: A review. *Prog. Org. Coat.*, 111, 175–185. DOI: 10.1016/j.porgcoat.2017.05.018.

Zhang A., Zhang Y., Zhu Z., 2019. Thermal properties of Halloysite nanotubes (HNTs) intercalation complexes – A review. *E3S Web Conf.*, 131, 01055. DOI: 10.1051/e3sconf/201913101055.

Zhang A.B., Pan L., Zhang H.Y., Liu S.T., Ye Y., Xia M.S., Chen X.G., 2012. Effects of acid treatment on the physico-chemical and pore characteristics of halloysite. *Colloids Surf., A*, 396, 182–188. DOI: 10.1016/j.colsurfa.2011.12.067.

Zhang B., Guo H., Yuan P., Li Y., Wang Q., Deng L., Liu D., 2020a. Geopolymerization of halloysite via alkali-activation: Dependence of microstructures on precalcination. *Appl. Clay Sci.*, 185, 105375. DOI: 10.1016/j.clay.2019.105375.

Zhang Y., Li Y., Zhang Y., 2020b. Preparation and intercalation structure model of halloysite-stearic acid intercalation compound. *Appl. Clay Sci.*, 187, 105451. DOI: 10.1016/j.clay.2020.105451.

Zhao L., Zhang Y., Miao Y., Nie L., 2016. Controlled synthesis, characterization and application of hydrophobic calcium carbonate nanoparticles in PVC. *Powder Technol.*, 288, 184–190. DOI: 10.1016/j.powtec.2015.11.001.

Received 03 April 2022
Received in revised form 12 August 2022
Accepted 06 September 2022